Materials Science and Metallurgy Engineering, 2013, Vol. 1, No. 2, 13-21
Available online at http://pubs.sciepub.com/msme/1/2/1

DOI:10.12691/msme-1-2-1

Effect of Severe Plastic Deformation on Structure and Properties of Al-Mg-Si Alloy of 6060 Type

M. Bournane[1], A. Berezina[2], O. Davydenko[3], T. Monastyrska[2,*], O. Molebny[2], V. Spuskanyuk[3], A. Kotko[2]

[1]University of Quebec at Chicoutimi, Saguenay, Quebec, G7H-2B1, Canada
[2]G.V. Kurdyumov Institute for Metal Physics of the NAS of Ukraine, Vernadsky Blvd., Kyiv, Ukraine
[3]O.O.Galkin Donetsk Institute for Physics and Engineering of the NAS of Ukraine, R.Luxembourg Str., Donetsk, Ukraine
*Corresponding author: monast@imp.kiev.ua

Received December 30, 2012; Revised June 03, 2013; Accepted June 04, 2013

Abstract The possibility of changing the structure and properties of the wrought low-alloyed, inexpensive Al-Mg-Si alloy due to the use of different modes of severe plastic deformation (SPD) in combination with different types of thermal treatments both before and after SPD has been studied. It was shown that the use of SPD at room temperature for Al-Mg-Si alloy formed a heterogeneous deformation structure which is characterized by incomplete dynamic recrystallization. The average grain size decreased from 200–500μm to 300–500nm. SPD provoked the deformation-induced complete or partial dissolution of excess phases, regardless of the initial state of the alloy. This was accompanied by the formation of a supersaturated solid solution in the matrix. Grain refinement and substructure formation led to the increase of tensile strength from 207 to 391 MPa in the pre-aged samples, their elongation being reduced by 30%. The study of aging and thermal stability of the structures formed after SPD showed that the SPD processes were accompanied by the formation of microporosity which determined the limits of the accumulated strain ($\Sigma e \leq 5.1$) and the aging temperature ($T \leq 140$ ℃).

Keywords: *6060 alloy, severe plastic deformation, hydrostatic extrusion, equal-channel angular hydroextrusion, aging, dynamic recrystallization*

1. Introduction

Using the methods of severe plastic deformation (SPD) to obtain bulk nanostructured metals and alloys with submicrocrystalline (SMC, grain size d ~ 100-1000nm) and nanocrystalline (d <100nm) grain structure in connection with the development of new combined methods of hardening metals and alloys is one of the most important areas of modern materials science [1]. These materials have unique mechanical properties and are considered as promising structural and functional materials of the next generation of metals and alloys. Understanding the mechanisms of structural phase changes due to SPD of pure metals and alloys is important for predicting the degradation and the subsequent destruction of materials under external thermomechanical action.

Now it is believed that the mechanism of hardening of pure metals resulting from SPD is based on the refinement of grains and the non-equilibrium state of grain boundaries with a high level of local internal stresses near the boundaries. However, in some heterogeneous alloys, not only grain refinement during SPD, but the formation or the dissolution of secondary dispersed phases also affects mechanical properties. The effect of additional hardening or softening is observed, depending on the structural state of these phases in a wide range of deformation. For example, such effects were found in aging aluminium alloys after three-dimensional SPD [3,4,5].

The formation of a SMC structure in relatively inexpensive industrial aluminum alloys due to the use of these technologies can transform low-strength alloys into medium-strength and high-strength ones. Aging aluminium alloys with SMC structures can be used for producing heavy-duty castings with high performance.

The possibility of changing the structure and properties of the wrought low-alloyed, low-cost Al-Mg-Si alloy of 6060 type through the use of severe plastic deformation has been studied. The alloy has high plasticity, the ability for hot extrusion, and high corrosion resistance, which are excellent characteristics for various applications. The low strength of the alloy, however, is its main disadvantage. Of great interest is the search for additional methods of hardening of the alloy. The primary task of this research investigation has been to study the possibility of improving the mechanical properties of the alloy using various modes of severe plastic deformation in combination with different types of thermal treatments both before and after SPD.

2. Experimental

Wrought Al-Mg-Si alloy of 6060 type was chosen for investigation. Alloys of 6060 type are the basis of an important class of heat-hardenable wrought alloys. These alloys are inexpensive, and have a low alloying content of

1–2%, which is significantly less than that of widely used aluminum alloys of 2XXX type. The equilibrium phase diagram of the alloy is well studied. Quasibinary Al-Mg_2Si section is observed in the system when the ratio of Mg:Si is 1.73, where the compound Mg_2Si, or β-phase, located on the quasibinary section, is in equilibrium with the aluminium solid solution. Industrial wrought alloys contain 0.6-1.5% Mg_2Si, with a small excess of magnesium or silicon. Alloys are strengthened due to the precipitation hardening during the aging process as a result of the formation of metastable hardening β′′ and β′ phases, which have a coherent and a semicoherent relation with the matrix, respectively. The β′ phase has a hexagonal lattice with parameters $a = 0.705$ nm, $c = 0.405$ nm, and precipitates in the form of needles and rods. The equilibrium β phase has a cubic FCC structure, with parameter $a = 0.635$ nm. The investigated Al-Mg-Si alloy is one with the lowest volume fraction of Mg_2Si phase (0.6%) and, accordingly, exhibits the lowest hardening during aging of the 6XXX series alloys. The composition of the 6060 alloy is shown in Table 1.

Table 1. The composition of the studied alloy

Alloy	Concentration of elements (wt %)						
	Mg	Si	Fe	Cu	Ti	Mn	Zn
6060	0.59	0.50	0.31	0.06	0.032	0.037	0.06

Specimens of three series of the alloy, corresponding to different initial treatments were prepared to investigate the effect of structure of the initial state of the alloy on the SPD and the final properties of the alloy. The three series were as follows:

1) Series A – Homogenization at 560ºC for 12 hours;

2) Series B – Homogenization at 560ºC for 12 hours + Air Quenching from 480ºC + Aging at 185ºC for 6 hours + Natural Aging;

3) Series C – Re-quenching of the specimens of the B series from 480ºC + Aging at 185ºC for 6 hours.

A combined method of conventional hydrostatic extrusion (HE) and equal-channel angular hydroextrusion (ECAH) was used as the SPD technique. The general deformation route of the specimens was the following: HE + n-ECAH (where n is the number of passes) + HE. The number of passes during the ECAH was n = 1, 2, 4. The sequence of deformation, the values of the strain e after each stage and total accumulated strain are presented in Table 2.

Table 2. The sequence of deformation of the specimens of the A, B, C alloy series

Series	Specimen Code*	HE e	HE e	ECAH		HE e	HE e	Σe
				n	e			
A	A-0	1.0	0.3	–	–	0.5	1.0	2.8
	A-1	1.0	0.3	1	1.2	0.5	1.0	4.0
	A-2	1.0	0.3	2	2.3	0.5	1.0	5.1
	A-4	1.0	0.3	4	4.6	0.5	1.0	7.4
B	B-0	1.0	0.3	–	–	0.5	1.0	2.8
	B-1	1.0	0.3	1	1.2	0.5	1.0	4.0
	B-2	1.0	0.3	2	2.3	0.5	1.0	5.1
	B-4	1.0	0.3	4	4.6	0.5	1.0	7.4
C	C-0	1.0	0.3	–	–	0.5	1.0	2.8
	C-1	1.0	0.3	1	1.2	0.5	1.0	4.0
	C-2	1.0	0.3	2	2.3	0.5	1.0	5.1
	C-4	1.0	0.3	4	4.6	0.5	1.0	7.4

* The suffix after the series number in these codes represents the number of ECAH passes, n.

The method of equal-channel angular hydroextrusion (ECAH), first developed at the Donetsk Institute for Physics and Engineering, NASU, is a modified method of equal-channel angular pressing. ECAH technique (Figure 1) was proposed by Spuskanyuk et al. for the processing of lengthy billets (l/d≥10) in [6]. Cylindrical billets were extruded from the container by a high-pressure fluid through an angular die with an angle Φ=90º (Figure 1). Deformation was realized at room temperature under the pressure of 150MPa for HE and 700MPa for ECAH.

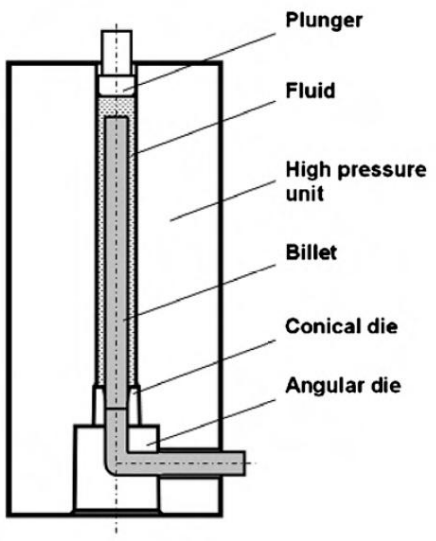

Figure 1. Schematic of the ECAH technique.

The effect of SPD on the aging of the 6060 alloy has been studied.

The structure of the alloys in the initial state, after SPD and aging was studied using transmission electron microscopy (JEM-2000FXII), volumetry, and Vickers Hardness measurements. The temperature intervals of the phase transformations were determined by measuring of the temperature coefficient of resistivity $\alpha_t = 1/\rho_0 \, d\rho/dT$.

3. Results and Discussion

3.1. The Structure and Properties of the 6060 Alloy in the Initial State

Specimens in the homogenized state (series A) and after aging (series B) were studied. Mechanical properties of the specimens after the initial treatment are presented in Table 3.

Table 3. Mechanical properties of the A and B series specimens after the initial treatment

Series	Treatment	Yield strength, MPa	Ultimate tensile strength, MPa	Elongation δ, %
A	Homogenization at 560ºC for 12h	86	116	22
B	Homogenization + Quenching from 480ºC + Aging at 185ºC for 6h	188	207	11

A TEM study of the alloys structure was carried out. Representative examples are shown in Figure 2. The rod-like coarse particles of the equilibrium β phase, ~200-600nm long and ~50-60nm thick, were present in the alloy in the homogenized state (Figure 2a). Precipitation density

of the particles is small; they are incoherent with the matrix and associated with dislocations. Fine needle-like particles of the metastable β′ phase, ~20nm long and ~5-6nm thick, were formed in the matrix after the decomposition of the supersaturated solid solution (Figure 2b). The particles had a high precipitation density, and were coherently bound with the matrix. These strengthening precipitates allowed improving to nearly double the strength of the alloy.

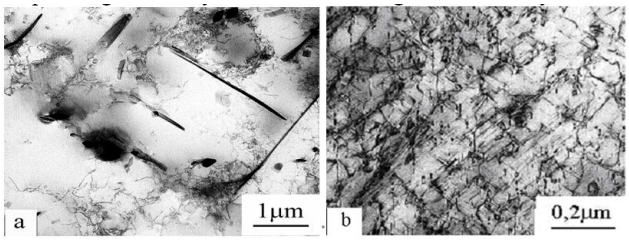

Figure 2. The structure of the 6060 alloy in the state before SPD: a) A series; b) B series

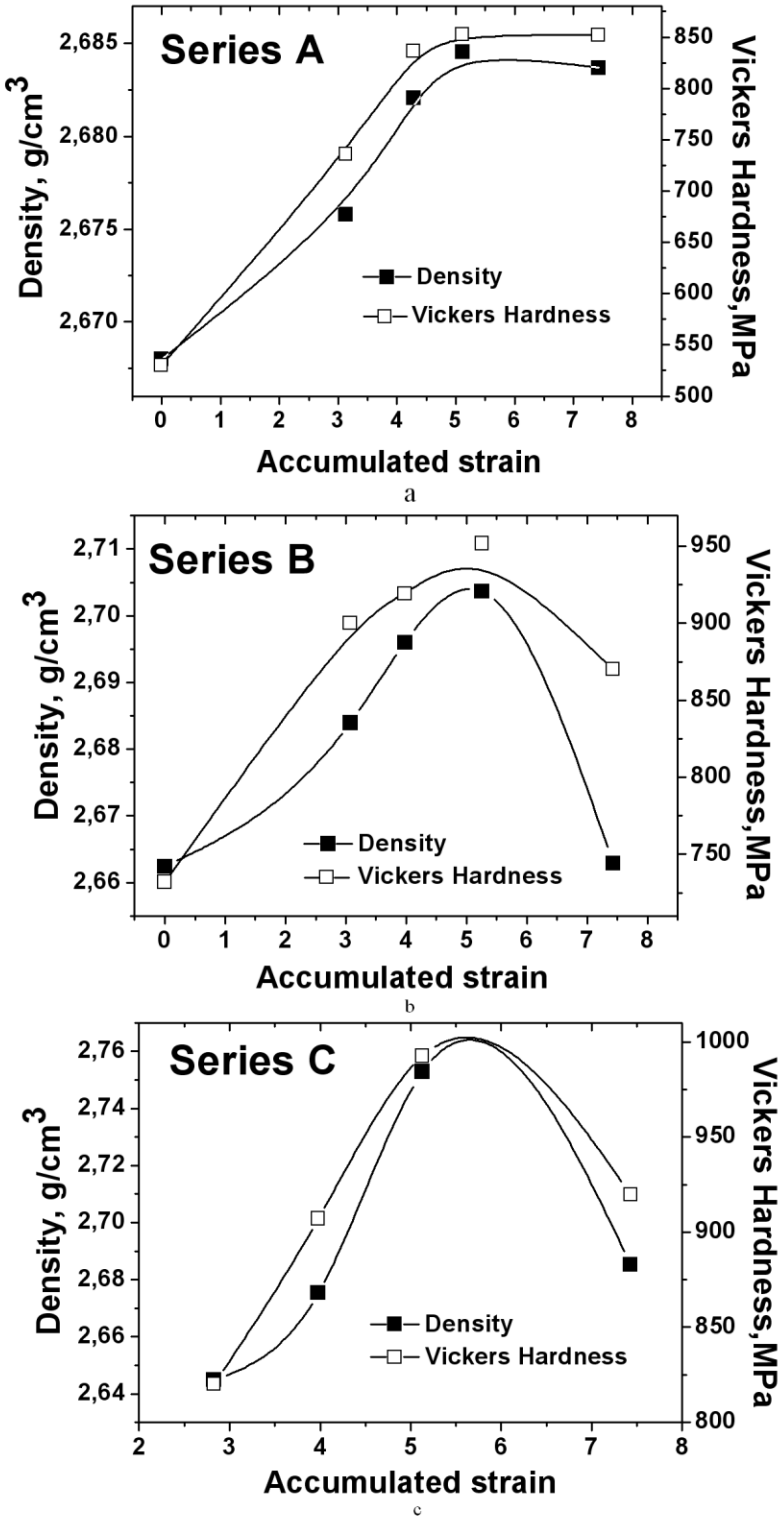

Figure 3. Correlation of changes in the Vickers Hardness and density of alloy specimens depending on the accumulated strain for (a) A, (b) B, and (c) C series

3.2. The Structure and Properties of the 6060 Alloy in the Initial State

Density and hardness were measured for all the states of the alloy with the finite value of Σe (Table 2). The data obtained are presented in Figure 3. It should be pointed out that the correlation between changes in density and hardness is observed during the increase of cumulative strain. For homogenized specimens (A series) the curves reached saturation, but for aged samples (B and C series) the density and hardness decreased after the accumulation of strain to Σe=5. Mechanical properties of these specimens are presented in Table 4.

The maximum value of ultimate tensile strength (UTS) was observed for aged specimens. For example, for specimens of B-2 series (accumulated strain Σe=5.1), UTS increased from 207MPa in the initial aged state to 391MPa, i.e., by almost 90%. However, the elongation to failure δ decreased from 11% to 7.6%. For homogenized specimens of the A-4 series (accumulated strain Σe=7.4), UTS increased from 116MPa in the initial state to 351MPa, whereas the elongation decreased from 22% to 6.1%.

Table 4. Mechanical properties of specimens of the A, B, C series after SPD

Specimen Code	Ultimate tensile strength, MPa	Hardness MPa	Elongation δ, %
A-0	272	736	8.1
A-1	307	836	7.1
A-2	309	853	9.5
A-4	351	853	6.1
B-1	364	919	7.2
B-2	391	952	7.6
B-4	335	870	6.6
C-0	263	820	11.6
C-1	302	907	6.6
C-2	384	993	7.5
C-4	331	920	6.1

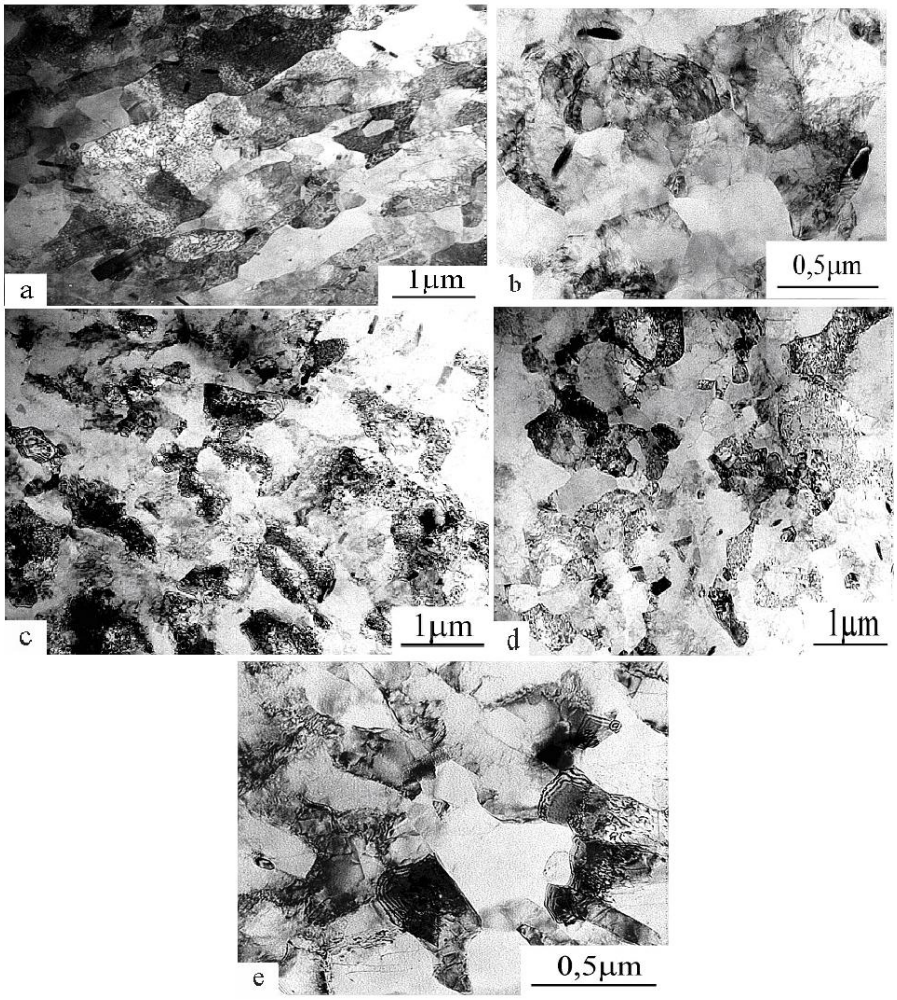

Figure 4. The effect of SPD on the structure of the A series specimens: (a, b) A-0; (c) A-1; (d) A-2; (e) A-4

The structures shown in Figure. 4 and Figure 5 are heterogeneous, and exhibit recrystallized and nonrecrystallized grains. Some regions of incomplete dynamic recrystallization may also be observed.

The fragmentation of the grain structure, from 200–500μm to 0.3–0.5μm, and the appearance of elongated recrystallized and nonrecrystallized grains are observed in the A-0 specimen after hydrostatic extrusion (cf. Figure. 4a and Figure 4b). A netlike dislocation structure is present inside the nonrecrystallized grains. Deformation-induced dissolution of the particles of the equilibrium - phase takes place. The particle size is reduced compared to that of the initial state: the length to 100nm, and the thickness to 20nm. The particles are mainly located on the grain boundaries (Figure 4b). Electron-diffraction analysis (Figure 6a-b) revealed that after this treatment the reciprocal lattice reflections are characterized by an azimuthal extension, which indicates the formation of the substructure.

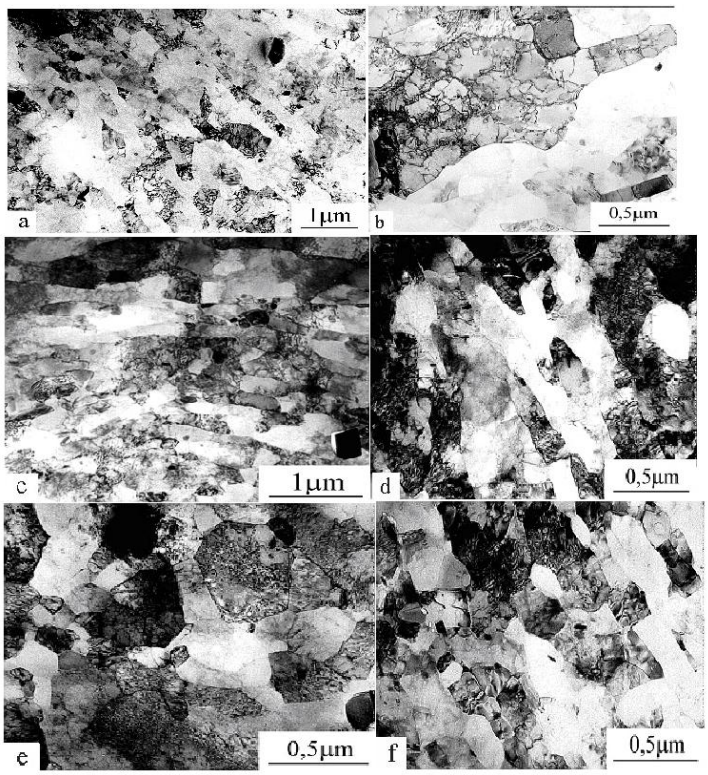

Figure 5. The effect of SPD on the structure of the C series specimens: (a, b) C-0; (c, d) C-1; (e) C-2; (f) C-4

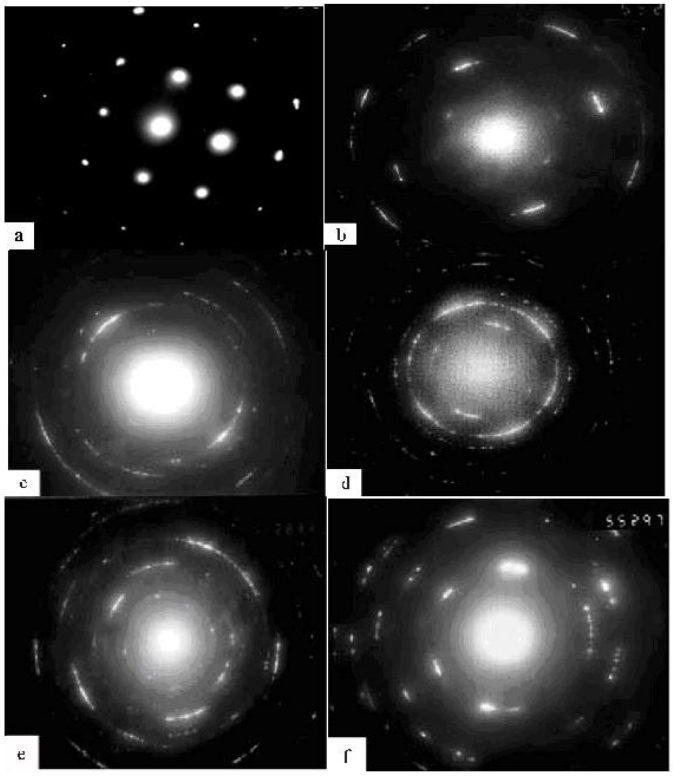

Figure 6. (a) the quenched alloy in the initial state; (b) A-0; (c) A-2; (d) C-2; (e) B-2 after aging at 140ºC for 1 hour; (f) B-2 after aging at 200ºC for 3 hours. ED patterns showing evolution of the alloy structure after SPD

Areas surrounded by the shell, which contains a netlike dislocation structure, appear in the matrix after ECAH when n=1 (A-1) (Figure 4c). Particles of the equilibrium β-phase are observed. The increase in the number of passes to n=4 (A-4) resulted in the formation of an alternating chain structure of recrystallized and nonrecrystallized grains (Figure 4e). β-phase particles are not observed. A well-developed substructure is formed after hydrostatic extrusion of aged specimens (C-0), as may be seen from Figure 5a-b. β-phase particles in the C-0, C-1, C-2 series specimens are not observed. β-phase particles appear after increasing the accumulated strain to $\Sigma e=7.4$ (Figure 5 f).

The comparison of the structural changes after SPD for homogenized specimens (A series) and aged specimens (C series) has shown that in the aged samples the processes of

structure formation are accelerated (Figure 4, Figure 5 and Figure 6 c-d).

3.3. The Effect of SPD on the Aging of the 6060 Alloy

To determine the ability for dispersion hardening of the alloy after SPD, the study of the temperature coefficient of resistivity, α_T, during continuous heating at the rate of 3°/min in the temperature range 20–400°C was carried out, besides hardness change isochrones in the temperature range of aging 20–200°C for all deformed specimens and isotherms HV=f(τ) at temperatures of 120°C, 140°C and 200°C, respectively, for B-2, B-1, B-4 specimens were plotted.

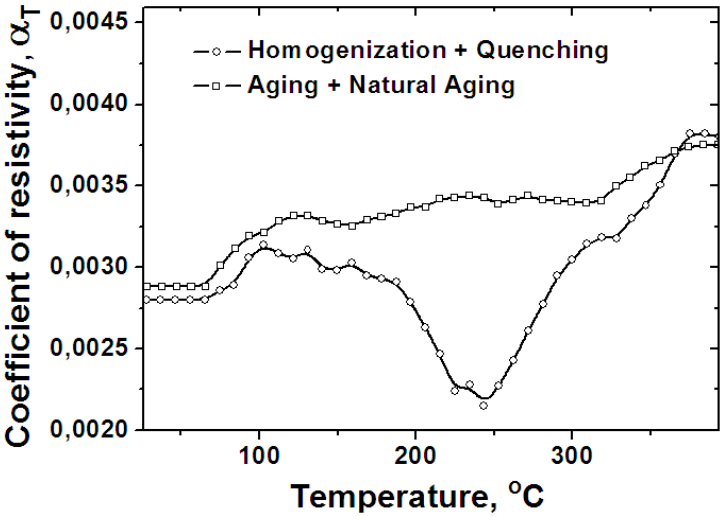

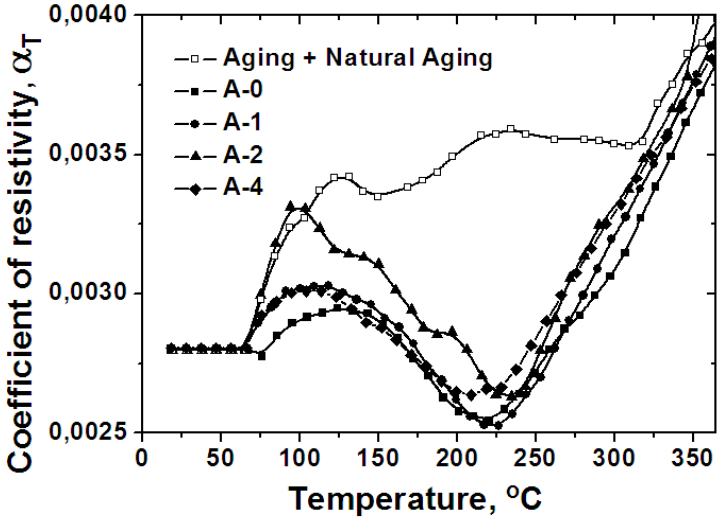

b

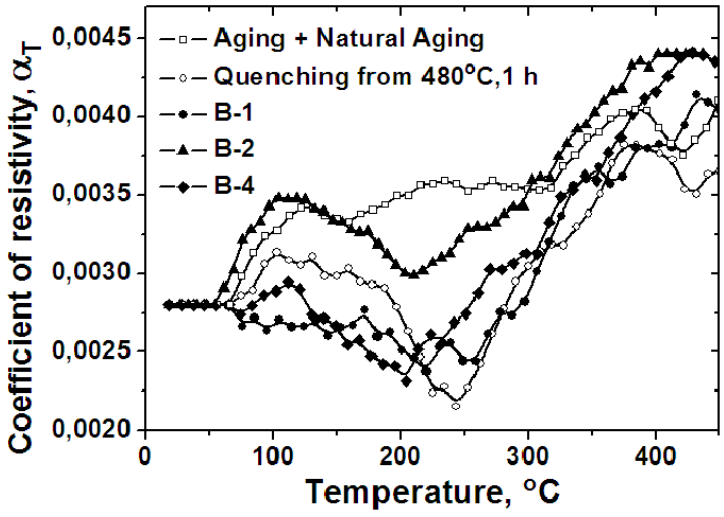

c

Figure 7. The change of αT = f(T) for (a) specimens without SPD, and specimens corresponding to (b) A series, (c) B series

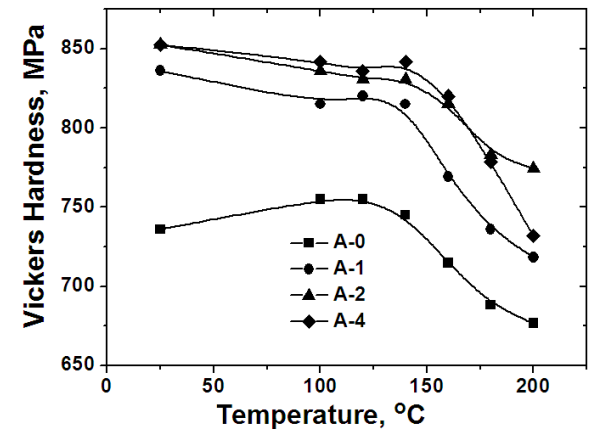

a

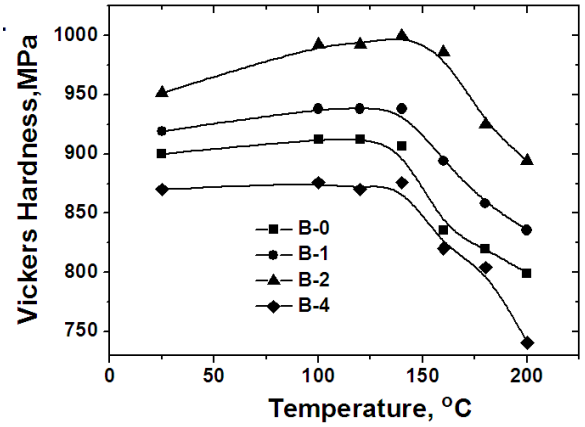

b

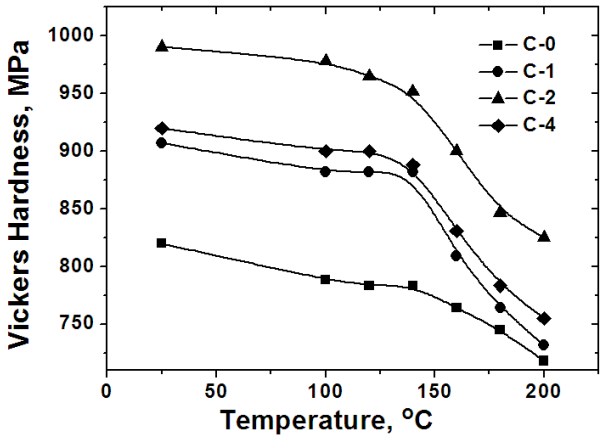

c

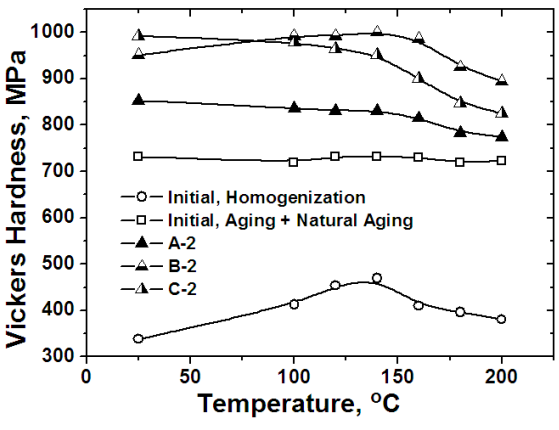

d

Figure 8. The change of hardness during isochronal annealing for 30 minutes after SPD of: A (a), B (b), C (c) series specimens; and the effect of preliminary heat treatment on the change of hardness (d)

The changes in α_T for homogenized, quenched and aged samples without SPD are shown in Figure 7a. The change of α_T=f(T) implies that its minimum is observed in the temperature range ~175ºC–325ºC for the quenched state (maximum supersaturation of solid solution). No minimum is observed for the aged state. For all states after SPD the minima of curves α_T=f(T) were observed (Figure 7b-c), therefore, the solid solution was supersaturated. The maximum supersaturation was observed for homogenized specimens.

For homogenized specimens, Figure 8, the maximum hardness is observed at the maximum accumulated strain in the A-4 specimen, the minimum hardness after HE in the A-0 specimen. A plateau or a slight increase in the curve HV=f(T) is seen in the temperature range 100ºC–140ºC.

For the artificially aged specimens of the C series, as well as for the A series, the minimum hardness is observed after hydrostatic extrusion and the maximum - for the C-2 specimen (Figure 8c).

For specimens of B series, the minimum hardness is observed in the B-4 specimen which has the maximum accumulated strain, and the maximum hardness - in the B-2 specimen (Figure 8b). This series demonstrates the most hardening.

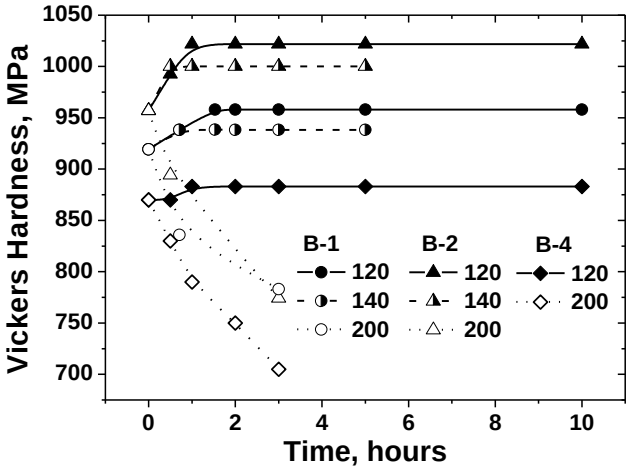

Figure 9. Hardness change during the isothermal aging of B series specimens

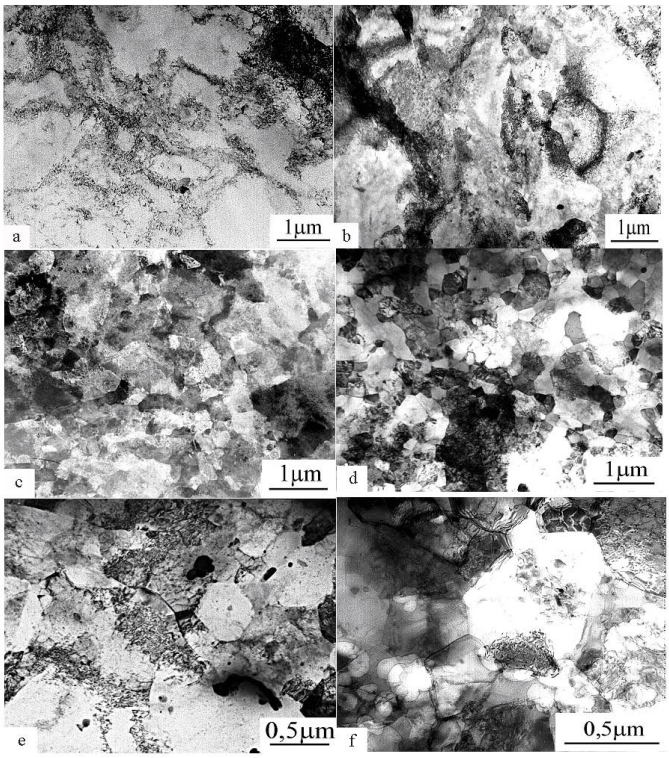

Figure 10. The structure of B series specimens after (a-d) aging at 140ºC for 1 hour: (a) B-0; (b) B-1; (c) B-2; (d) B-4; and (e-f) aging at 200 ℃ for 3 hours; (e) B-2; (f) B-4

Comparison of isochrones for the specimens after SPD and without SPD (Figure 8d) shows that the aged state without SPD is the most thermally stable. The highest-strength state is observed after SPD (B-2), but the thermal

stability of all specimens after SPD becomes worse after aging at 150°C.

The hardness changes during isothermal aging at 120°C, 140°C and 200°C were analyzed for the highest-strength B series, as shown in Figure 9. The initial rise of hardness at 120°C and 140°C is observed after 1-2 hours of aging, and remains unchanged with further increase in aging time. A loss of hardness is observed after increasing aging temperature to 200°C.

The evolution of structure during the aging of the alloy after SPD is shown in Figure 10 for specimens of the B series. The developed substructure (Figure 5 a-b) is replaced by a cellular dislocation structure after aging at 140°C for 1 hour of specimens after HE (Figure 10a); the elongated chain-like structure disappears after ECAH and aging at 140°C (Figure 10 b-d). The electron diffraction pattern shown in Figure 6d and Figure 6e confirms the coarsening of the grain structure and the disappearance of the substructure. Stable β and metastable β′ phases present in the alloy are spherical-shaped.

Increasing of the aging temperature up to 200°C leads to further coarsening of the structure (Figure 6f, Figure 10e). Increasing of the accumulated strain up to the maximum value Σe=7.4 is accompanied by formation of pores of 100-200 nm size in the matrix (Figure 10f). Rodlike β phase particles are found very rarely in the alloy. A bimodal distribution of equiaxed β phase particles with average sizes of 40-50 nm and 10-15nm is mainly observed in the matrix.

The correlation between the change of hardness and density of the alloy (Figure 3), as well as the development of porosity during the aging of alloy after SPD with Σe=7.4, indicates that the SPD processes are accompanied by the formation of microporosity, which determines the extreme values of accumulated strain and temperature aging.

4. Conclusions

1. The use of SPD at room temperature for 6060 alloy produced a heterogeneous deformation structure which consisted of recrystallized and nonrecrystallized grains and showed incomplete dynamic recrystallization. The average grain size decreased from 200-500 μm to 300-500 nm. The increase in accumulated strain led to the formation of a chain-like structure consisting of alternating recrystallized and nonrecrystallized grains.

2. The effect of genetic structure of the material in the initial state on the hardness and density change of the alloy as a function of accumulated strain was determined. It was shown that the higher degree of strain without the decrease of hardness was achieved for the homogenized alloy than for the aged one.

3. The study of the changes in the temperature coefficient of resistivity showed that supersaturation of alloying elements of the matrix was observed after SPD regardless of the initial state of the alloy, which was attributed to the deformation-induced complete or partial dissolution of the β and β′ phase particles present in the matrix.

4. The analysis of the change in hardness during isochronal aging showed that maximum hardness was obtained in specimens of B series with accumulated strain Σe=5.1. The increase in the degree of strain of the specimens to Σe=7.4 led to the greatest decrease in hardness after aging, which resulted from intense pore formation in the matrix.

5. TEM study of aging of supersaturated solid solutions after SPD showed that the β phase precipitated mainly at the grain boundaries discontinuously. The morphology of the precipitated phase varied from rod-like to the equiaxed. Finely dispersed β phase particles that were precipitated continuously had a low volume fraction and did not contribute significantly to the strengthening of the alloy.

6. The study of aging and thermal stability of the structures formed after SPD showed that the SPD processes were accompanied by the formation of microporosity which determined the limits of the accumulated strain (Σe≤5.1) and the aging temperature (T≤140°C). The thermal stability of specimens after SPD was lower than that without the use of SPD.

7. Grain refinement and substructure formation obtained after SPD in the pre-aged specimens of B-2 series after SPD led to the increase of tensile strength from 207 to 391 MPa with the accumulated strain Σe=5.1, their elongation being reduced by 30%. For homogenized specimens of A-4 series after SPD with Σe=7.4 tensile strength increased up to 351 MPa, three times as much compared to the original homogenized state, and the elongation decreased from 22% to 6.1%.

References

[1] Valiev, R.Z., Langdon, T.G., "Principles of equal-channel angular pressing as processing tool for grain refinement," *Progress in Materials Science*, 51. 881-981. 2006.

[2] Sitdikov, O., Sakai, T., Avtokratova, E., Kaibyshev, R., Kimura, Y., Tsuzaki, K., "Grain refinement in a commercial Al–Mg–Sc alloy under hot ECAP conditions," *Mater. Sci. Eng. A*, 444. 18-30. 2007.

[3] Szczygiel, P., Roven, H.J., and Reiso, O., "On the effect of SPD on recycled experimental aluminium alloys: Nanostructures, particle break-up and properties," *Mater. Sci. Eng. A*, 410-411. 261-264. 2005.

[4] Gubicza, J., Schiller, I., Chinh, N.Q., "The effect of severe plastic deformation on precipitation in supersaturated Al–Zn–Mg alloys," *Mater. Sci. Eng. A*, 460-461. 77-85. 2007.

[5] Vidal, V., Zhang, Z.R., and Verlinder, B., „Precipitation hardening and grain refinement in an Al–4.2wt%Mg–1.2wt%Cu processed by ECAP," *J. Mater. Sci.*, 43. 7418-7425. 2008.

[6] Spuskanyuk, V., Davydenko, O., Berezina, A., et al., "Effect of combining the equal-channel angular hydroextrusion, direct hydroextrusion and drawing on properties of copper wire," *Journal of Materials Processing Technology*, 210. 1709-1715. 2010.